





Article

A New Cross-Flow Type Turbine for Ultra-Low Head in Streams and Channels

Calogero Picone ¹, Marco Sinagra ^{2,*}, Luana Gurnari ¹, Tullio Tucciarelli ² and Pasquale G. F. Filianoti ¹

¹ Department of Civil, Energy, Environmental and Material Engineering (DICEAM), University Mediterranea of Reggio Calabria, 89124 Reggio Calabria, Italy

² Department of Engineering, University of Palermo, 90128 Palermo, Italy

* Correspondence: marco.sinagra@unipa.it

Abstract: In the last few decades, hydropower production has been moving toward a new paradigm of low and diffused power density production of energy with small and mini-hydro plants, which usually do not require significant water storage. In the case of nominal power lower than 20 kW and ultra-low head H ($H < 5$ m), Archimedes screw or Kaplan type turbines are usually chosen due to their efficiency, which is higher than 0.85. A new cross-flow type turbine called Ultra-low Power Recovery System (UL-PRS) is proposed and its geometry and design criteria are validated in a wide range of operating conditions through 2D numerical analysis computed using the ANSYS Fluent solver. The new proposed solution is much simpler than the previously mentioned competitors; its outlet flow has a horizontal direction and attains similar efficiency. The costs of the UL-PRS turbine are compared with the costs of one Kaplan and one cross-flow turbine (CFT) in the case study of the main water treatment plant of the city of Palermo in Italy. In this case, the UL-PRS efficiency is estimated using a URANS 3D numerical analysis computed with the CFX solver.

Keywords: cross-flow turbine; hydropower; sustainable energy; ultra-low head turbine



Citation: Picone, C.; Sinagra, M.; Gurnari, L.; Tucciarelli, T.; Filianoti, P.G.F. A New Cross-Flow Type Turbine for Ultra-Low Head in Streams and Channels. *Water* **2023**, *15*, 973. <https://doi.org/10.3390/w15050973>

Academic Editors: Xiangyu Hu and Wencheng Guo

Received: 18 January 2023

Revised: 22 February 2023

Accepted: 28 February 2023

Published: 3 March 2023



Copyright: © 2023 by the authors. Licensee MDPI, Basel, Switzerland. This article is an open access article distributed under the terms and conditions of the Creative Commons Attribution (CC BY) license (<https://creativecommons.org/licenses/by/4.0/>).

1. Introduction

Hydropower plants are traditionally classified, according to the nominal power P of the turbine, into large ($P > 100$ MW), medium (100 MW $> P > 15$ MW), small (15 MW $> P > 1$ MW), mini (1 MW $> P > 100$ kW) and micro (100 kW $> P > 5$ kW) hydro plants [1]. In the last few decades, small and mini new hydro plants have mainly been constructed. This is also due to the search for low, diffused power density production of energy, but the main reason is that medium and large hydro plants are usually associated with water storage in large artificial reservoirs. The construction of new water reservoirs is often blamed for a bad environmental impact, mainly due to the induced reduction of solid transport [2], as well as the change occurring in the downstream river hydrological regime [3,4] and loss of water due to evaporation [5].

Small and mini hydro-plants do not require significant water storage upstream of the turbine. These types of hydro-plants can work with both action and reaction turbines. Action turbines with free discharge, such as Pelton or cross-flow ones, are usually simpler and allow a short payback time, even with a small available nominal power. Turbines with a pressurized diffuser and positive outflow pressure, such as Francis and Kaplan ones, are more expensive but allow use of the entire available hydraulic jump, whereas turbines with free discharge need to leave the height between the horizontal axis of the turbine and the downstream water level unexploited (see Figure 1). This distance is usually small with respect to the total jump but can become significant with low and ultra-low head jumps. In this range, the kinetic energy of part of the flow of tidal currents can be converted into electricity by using kinetic turbines, where a converging duct is applied before the turbine to increase the total amount of intercepted energy. In this case, it is possible to compare the efficiency of different devices using the power coefficient defined in [6].

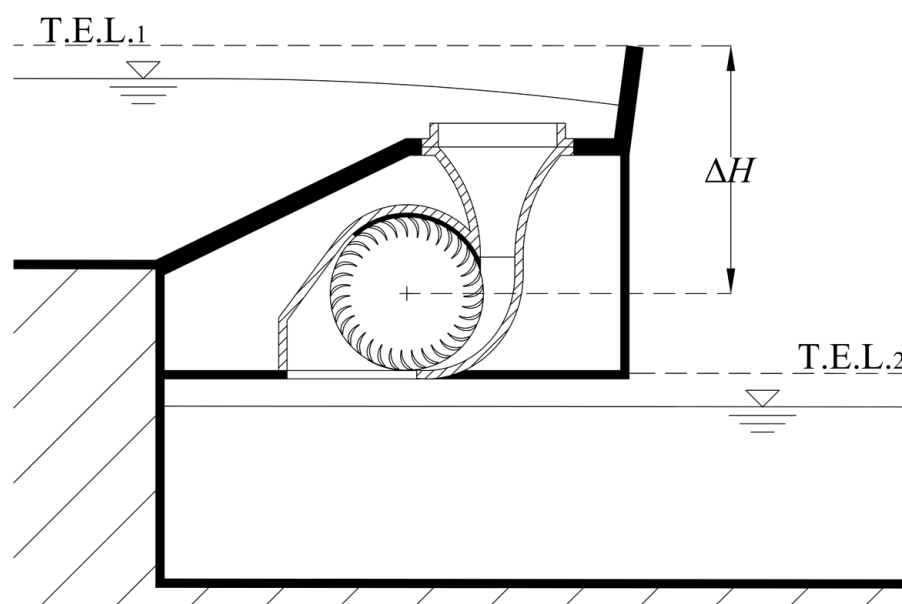


Figure 1. Typical installation of a traditional cross-flow turbine where T.E.L. both time is the total energy level in the upstream and downstream channels, and ΔH is the usable hydraulic jump, lower than the entire available one.

Other suitable locations for low head turbines are small weirs or natural/artificial bed jumps available in small channels, where the entire flow rate can be turbinized. In this case, some authors have proposed variants of Francis and Kaplan type turbines, such as a siphon hydro turbine [7] and a hydraulic propeller turbine [8], but at the present time, these solutions have complex geometries and their cost could not be competitive in micro hydro plants.

The Power Recovery System (PRS) is a cross-flow type turbine with positive outflow pressure [9–13]. Cross-flow and PRS turbines have been tested and applied, up to now, mainly to hydropower plants with medium head jumps greater than 15 m and smaller than 100 m. For higher heads, a new cross-flow type turbine called H-PRS has also been proposed [14] to fill a technological void that exists at the present time for hydropower production inside pipes, where large head drops and small discharges are available, especially if the discharge has large temporal variability. For lower head jumps, Kaplan type turbines attain efficiency higher than 85% and are traditionally assumed to be the most efficient ones. In the following, we will show that it is also possible to achieve similar efficiency with a new PRS type turbine, named UL-PRS. The advantage of using PRS type turbines is that they have simpler geometry and their cost could be, for the same nominal power, much lower than the cost of Kaplan turbines.

In the following sections, after a short review of the PRS turbine design criteria, the UL-PRS turbine is proposed and a sensitivity analysis of its efficiency with respect to the head jump is carried out. Finally, a UL-PRS prototype is designed for a potential site in the main wastewater treatment plant (WWTP) of the city of Palermo. The same cost/benefit analysis is applied to the selected case study for the UL-PRS and for other possible competitors [15].

2. PRS Turbine Design for Ultra-Low Hydraulic Heads

PRS is an inline turbine with a mobile flap for hydraulic regulation, a pressurized diffuser and the same runner as the cross-flow turbine (Figure 2). The design procedure for the PRS can be divided into two steps. The first step is the design of the runner, i.e., rotational velocity ω , diameter D , width W , blade thickness t and number of blades N_b . The second step is the stator design, i.e., nozzle and diffuser.

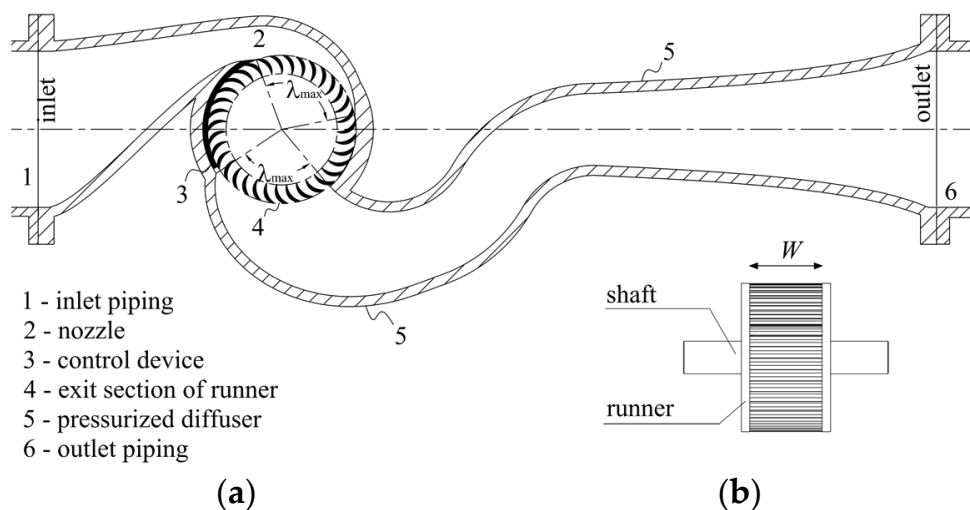


Figure 2. PRS turbine for medium head jumps: (a) Section view of the turbine in a symmetry plan; (b) Side view of the rotor [9,13].

In the case of an ultra-low hydraulic head, i.e., $\Delta H \leq 3$ m [7], the traditional PRS diffuser still provides good efficiency values but has a vertical outlet flow and shows a sharp efficiency reduction close to the minimum head values. See in Figure 3 the efficiencies computed with several PRS machines designed using different head values, but the same flow rate ($Q = 0.840$ m³/s), the same velocity ratio ($V_r = 1.8$) and the same rotor outer diameter ($D = 913$ mm). The efficiencies are defined as follows [14]:

$$\eta = \frac{P}{\gamma \cdot Q \cdot \Delta H} \tag{1}$$

where P is the produced mechanical power, γ is the water specific weight, ΔH is the difference between the Total Energy Level (T.E.L.) of the inlet channel and the T.E.L. of the discharge channel (Figure 4). T.E.L. is the entire energy per unit weight of the flow, obtained as the sum of the piezometric level and the kinetic energy terms.

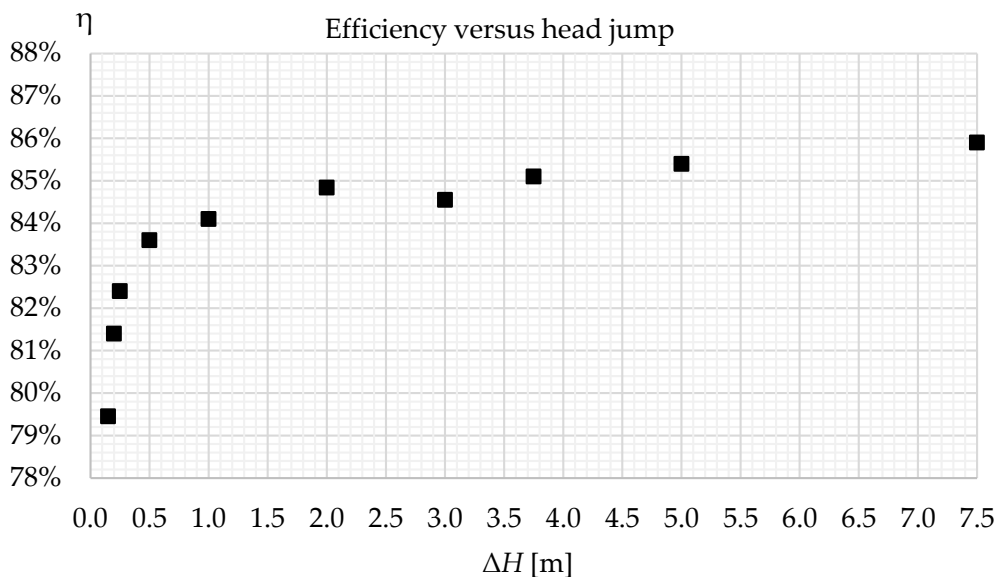


Figure 3. Efficiencies versus head jumps solved using 2D CFD analysis.

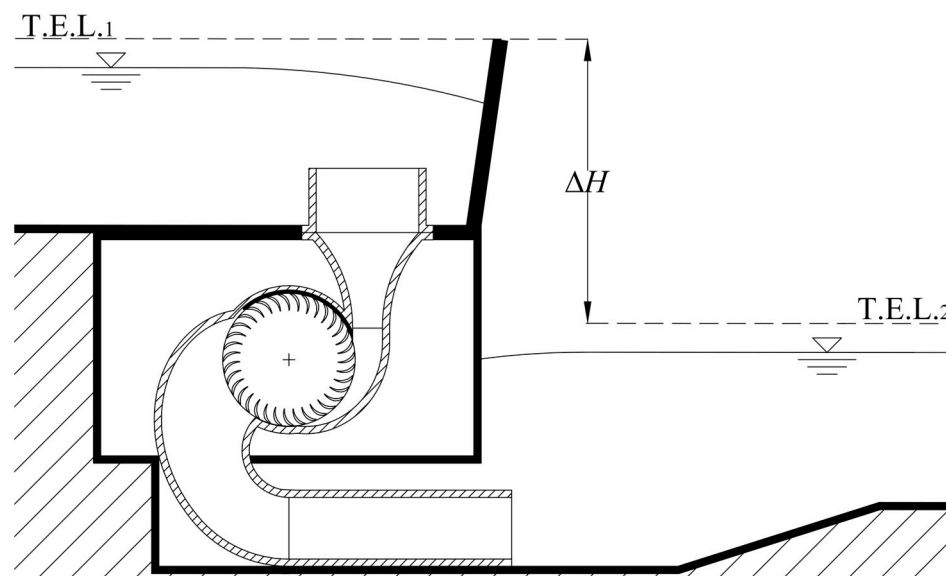


Figure 4. Section view of the UL-PRS turbine in a symmetry plan: T.E.L. is the total energy level and ΔH is the gross available hydraulic jump.

The reason for the sharp efficiency reduction is likely to be that the pressure differences inside the rotor of a cross-flow type turbine are usually small with respect to the kinetic energy resulting from the energy transformation inside the nozzle but become significant in the case of low ΔH . In this case, the angle of the flow direction with respect to the gravity force direction became quite important in the machine design. For this reason, this paper presents a new cross-flow type turbine, named UL-PRS (Figure 4), equipped with a new diffuser that makes it possible to keep the hydraulic efficiency above 80%, even with a hydraulic head drop of a few hundred millimeters and has a horizontal outflow direction (see Figure 4).

The UL-PRS design can be divided into two steps. The first is the design of the rotor and nozzle of the UL-PRS turbine, which is basically the same as the previous PRS and is fully described in [9–13].

The second step is the design of the pressure diffuser, which is composed of three parts. The first part (*I* in Figure 5) was designed according to the following hypothesis (see Figure 6): the runner outlet velocity only has radial component V_2 , which is constant along all the runner outlet circus; the velocity component on the direction normal to any radius of the runner normal to the axis is constant inside part *I* [16] and its module is equal to V_2 ; the two lateral walls are planar and their distance is equal to W , the width of the runner. According to these hypotheses, the flux V_2 per unit rotor outlet area can be obtained from the mass conservation equation as follows:

$$V_2 = \frac{2Q}{W \cdot D \cdot \lambda_{max}} \quad (2)$$

The radial distance r of the profile of the external wall of the diffuser from the axis of the rotor is a function of the λ angle and equal to:

$$r(\lambda) = \frac{D}{2}(1 + \lambda) \quad (3)$$

and the maximum height S_{max} of the diffuser cross-section in part *I* is equal (Figure 6):

$$S_{max} = \frac{D}{2} \lambda_{max} \quad (4)$$

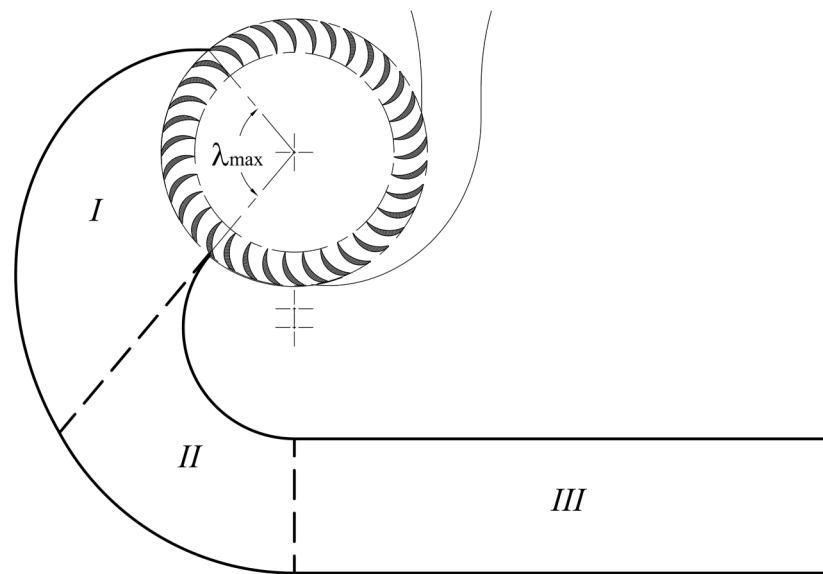


Figure 5. Section view of the diffuser, composed of parts marked I, II and III.

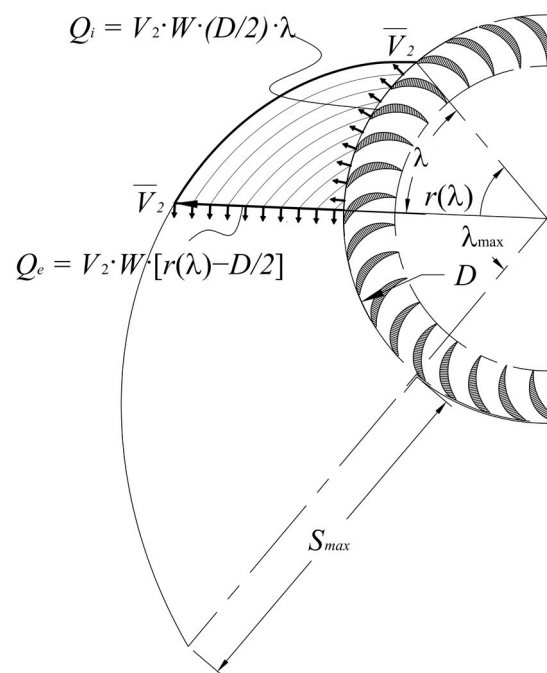


Figure 6. Section view only of the first diffuser part.

In the second part of the diffuser (II in Figure 5), the height of the rectangular cross-section decreases to prevent the generation of vortices because of path curvature changes. The width of this part remains constant and is equal to W . The final cross-section is vertical, its height is set equal to R (Figure 7) and the tangent at the final point of the two profiles is horizontal.

The curvatures of the inner and outer profiles are constant and their values are computed from the known position of the initial and final points and of the corresponding tangent directions.

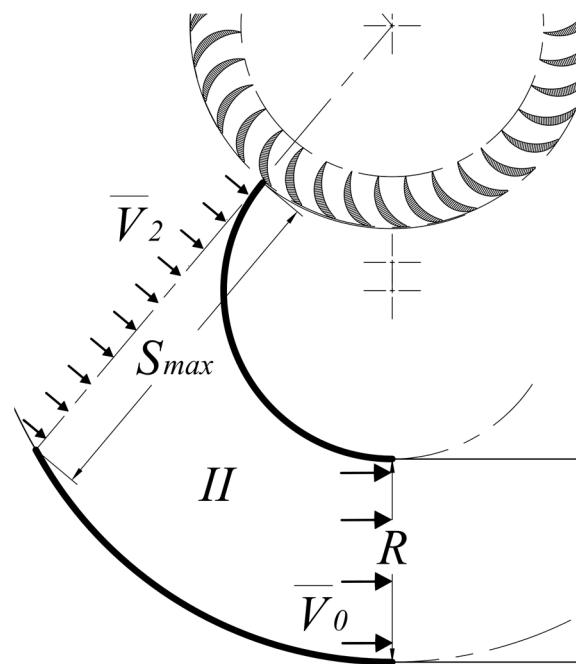


Figure 7. Section view of the second diffuser part.

The last part of the diffuser, marked as III in Figure 5, is a straight divergent duct with a fixed height equal to R (Figure 8). The axial velocity component in a generic cross-section is assumed to change linearly, with a corresponding hyperbolic growth of the cross-section area [17], according to:

$$V(l) = V_0 + k l \tag{5}$$

where V_0 is the initial velocity and l is the distance of the section from the beginning of part III. The distance of the last cross-section, l_{max} , is about 4 times R , a good compromise between the need to prevent the generation of vortices and to contain the overall length of the diffuser.

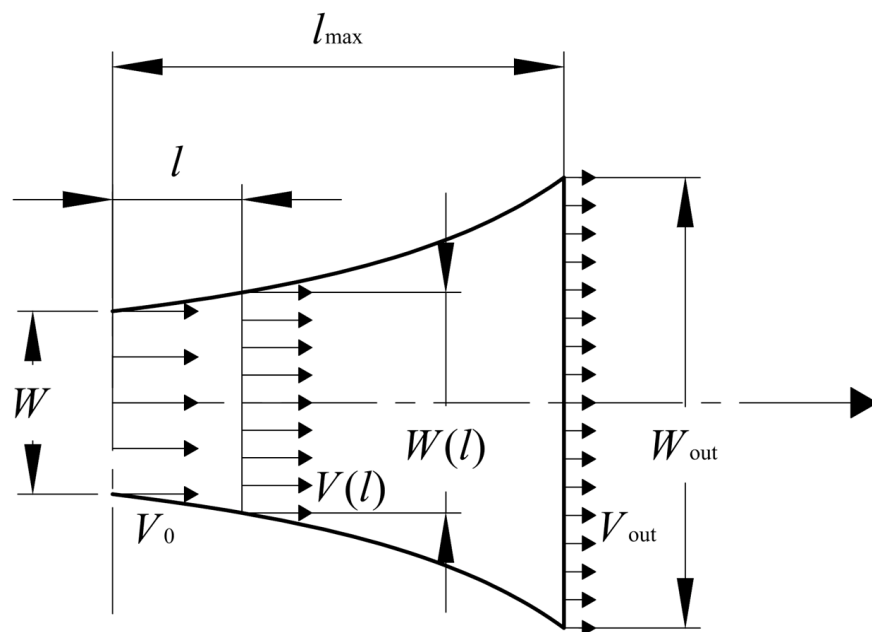


Figure 8. Top view of the last section of the diffuser.

The value of k in (5) and the maximum width W_{out} (Figure 8) are obtained by setting as V_{out} , the velocity of fluid particles at the exit of this last part of the diffuser, equal to 1 m/s, in order to get negligible final kinetic energy.

$$V_{out} = 1 \text{ m/s} \quad (6)$$

$$k = \frac{V_{out} - V_0}{l_{max}} \quad (7)$$

$$W_{out} = \frac{Q}{V_{out} R} \quad (8)$$

CFD Analysis of UL-PRS Turbine

We tested the new design procedure using both 2D and 3D computational fluid dynamics (CFD), the former of which compared the behavior of many different geometries. Due to the planar symmetry of its runner and distributor, the difference between the 2D and 3D solutions of a PRS turbine is usually small [16]. Although the efficiency calculated with 2D models is higher than the efficiency obtained with both 3D models and experimental data, this difference does not affect the optimality of the 2D parameters because the reduction of efficiency is not dependent on their setting and the optimal configuration is the same for both models [13]. The 2D analyses are much faster than the 3D ones, so we preferred to use the 2D approach for the research of optimal design and to limit the use of 3D analyses only to estimate the efficiency of the final geometry in a specific case study.

The numerical model was solved using ANSYS[®] CFX in the case of 3D domains and ANSYS[®] Fluent in 2D analyses. Following the experience of previous studies [12,13], the RNG k-epsilon model was selected as the turbulence model, combined with a scalable wall function [14]. For the study of rotating machines, both ANSYS[®] CFD solvers adopt a sliding mesh strategy, where the runner and its swept zone are discretized within a rotating reference system.

Fluent gives the option of selecting one among different approaches for pressure-based solving; we used the coupled one, where the whole set of momentum and continuity equations is solved simultaneously, resulting in strong coupling between pressure and velocity [18].

In CFX as the advection model, we chose the high-resolution scheme, which uses second-order differencing for the advection terms in flow regions with low variable gradients and uses the first-order advection terms only in areas where the gradients change sharply to prevent overshoots and undershoots and maintain robustness [14].

The effects of gravity are usually small with respect to the total jump in the traditional PRS but can become significant with low and ultra-low head jumps. For this reason, in both models, we enabled the gravity option under Gravity in Fluent or Buoyancy modes in CFX. When these settings are enabled, the solver increases the value of pressure p' up to the following value:

$$p = p' + (\rho - \rho_0)gy \quad (9)$$

where g is the norm of the gravitational acceleration, directed along the opposite direction of the vertical axis y in both models (Figure 9) and equal to 9.80665 m/s^2 , ρ is the density of the water, ρ_0 is the operating density and equal to 1.225 kg/m^3 , the density of air at $15 \text{ }^\circ\text{C}$.

The boundary conditions (BCs) selected in both 2D and 3D simulations are as follows: the total pressure, equal to the sum of the piezometric level and the kinetic energy terms per unit weight, at both the nozzle inlet and the outlet section of the casing for the static domain; module and direction of the angular velocity vector for the runner domain. All analyses were run for a simulation time corresponding to more than 6 full revolutions [16] and more than 200 time-steps per revolution in order to guarantee periodic, deterministic convergence of the model [14]. Previous studies have shown a very good match between the results of this numerical model and the experimental data [10,11]. A preliminary grid convergence analysis, aimed at assessing the minimum density of the mesh required to

get a negligible numerical error, has been carried out using steady state simulations and a maximum root mean square residual equal to 10^{-5} [13,14].

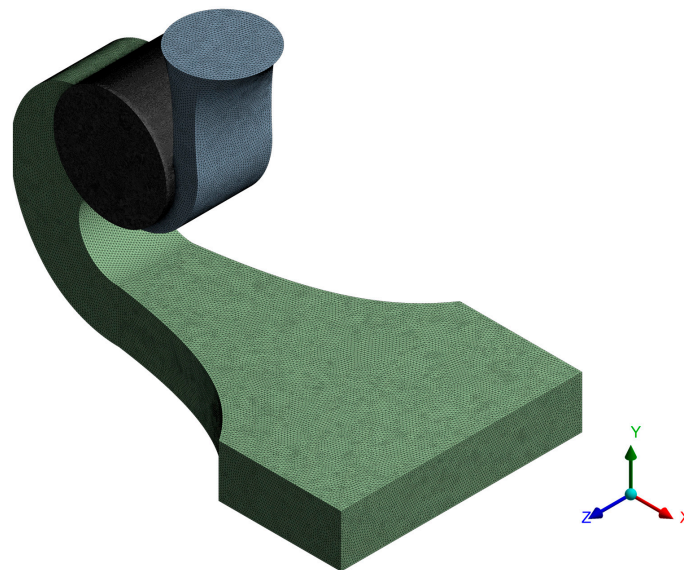


Figure 9. Trimetric view of the UL-PRS 1 3D Grid scheme.

In Table 1, the parameters of the convergence meshes used in both the 2D and 3D simulations are shown. Figure 9 shows the 3D mesh for UL-PRS 1.

Table 1. UL-PRS 1 and UL-PRS 2 convergence mesh details.

Parameters	UL-PRS 1		UL-PRS 2
Type of Domain	2D	3D	2D
Stator Domain elements	42,337	8,885,639	40,352
Rotor Domain elements	151,895	12,723,105	101,627
Total elements	194,232	21,608,744	141,979

A series of CFD 2D simulations were then performed. The geometrical parameters of the two different UL-PRS turbines are shown in Table 2. Both turbines were solved assuming the same flow rate Q , but the rotational velocity and width W were changed in each simulation to maintain the optimality conditions according to the different possible heads ΔH . The optimality conditions and the corresponding design criteria can be found in [9–13]. Observe that the blade maximum thickness t_{\max} in the last row is selected according to [13] to guarantee structural safety and maintain high hydraulic efficiency.

Table 2. UL-PRS 1 and UL-PRS 2 parameters.

Parameters	UL-PRS 1		UL-PRS 2
Flow rate Q [m^3/s]	0.840		
D [mm]	913		652
Head ΔH [m]	0.25–15		0.2–10
$\omega(\Delta H)$ [rpm]	19.4–150		24.3–171.6
$W(\Delta H)$ [mm]	2360–305		3695–523
α [$^\circ$]	15		15
β [$^\circ$]	28.2		28.2
λ_{\max} [$^\circ$]	100		100
N_b [-]	33		35
t_{\max} [mm]	22		15.7
η_{\max} [%]	87.5		87.1

The resulting efficiencies η versus heads ΔH are shown in Figure 10 along with the same values $\bar{\eta}$ normalized with respect to the maximum efficiency computed for each different geometry.

$$\bar{\eta} = \frac{\eta}{\eta_{max}} \tag{10}$$

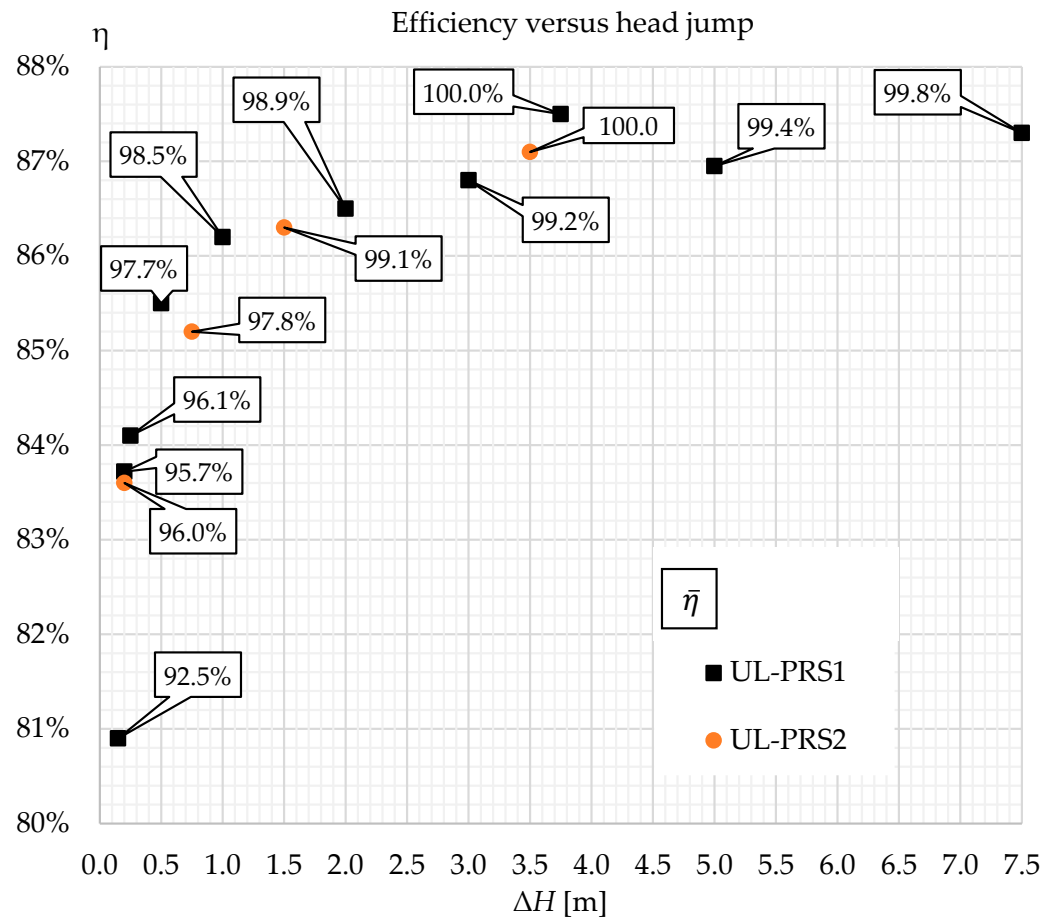


Figure 10. Sensitivity analysis of UL-PRS efficiency with respect to head jump.

Because we used 2D models, we expect the computed efficiencies to be higher than the efficiencies computed with 3D models or obtained from experimental data, but we can rely much more on the normalized values, also according to previous analyses [13]. We can observe an abrupt reduction in the normalized efficiencies for both turbines only for head drops lower than 0.5 m. The reason for such a reduction is likely to be that the kinetic energy at the rotor inlet becomes very small for extremely low water heads and is strongly dependent on the elevation of the single inlet point, in contrast with the design hypothesis. See in Table 3 a list of the efficiencies computed for both the PRS machines, shown in Figure 3, and the UL-PRS1 one, shown in Figure 10. All turbines are designed for the same flow rate ($Q = 0.840 \text{ m}^3/\text{s}$), velocity ratio ($V_r = 1.8$) and outer runner diameter ($D = 913 \text{ mm}$) and differ only for the nozzle axis orientation and the shape of the diffuser. The comparison clearly shows some advantages for the efficiencies of the UL-PRS turbine, mainly with head jumps lower than 3 m.

Table 3. Two-dimensional efficiency comparison between UL-PRS1 and PRS turbines for different head jumps.

Head ΔH [m]	UL-PRS 1	PRS
7.50	87.3%	85.9%
5.00	87.0%	85.4%
3.75	87.5%	85.1%
3.00	86.8%	84.6%
2.00	86.5%	84.8%
1.00	86.2%	84.1%
0.50	85.4%	83.6%
0.25	84.1%	82.4%
0.20	83.7%	81.4%
0.15	80.9%	79.5%

3. Case Study: Acqua Dei Corsari WWTP

The main wastewater treatment plant in the city of Palermo is the Acqua dei Corsari plant, located at the southeast end of the city (Figure 11). The WWTP is at an average altitude of 10 m above sea level and covers an area of approximately 110,000 m².

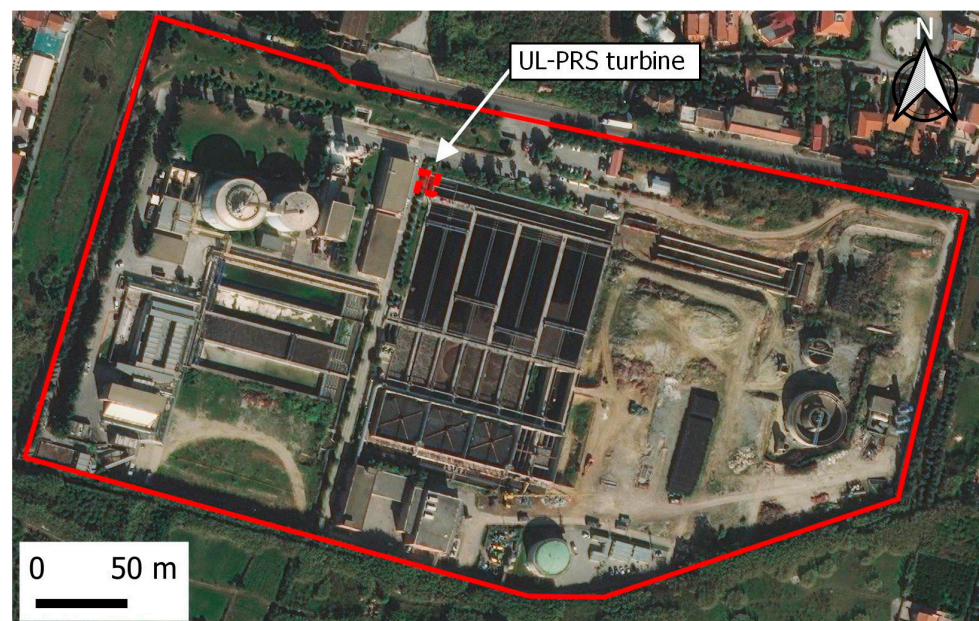


Figure 11. Acqua dei Corsari WWTP: Aerial view.

At present, the treated discharge Q is about 0.8 m³/s, corresponding to the wastewater produced by 320,000 equivalent inhabitants (EinH), and is expected to increase to 1.0 m³/s in two years, equal to the wastewater produced by about 400,000 EinH. A small head jump h_1 of about 3.5 m is present at the end of the disinfection channel (red area in Figure 11). The clarified water flow passes through two rectangular weirs and reaches the discharge channel. In the case of heavy rain events, part of the water at the entrance of the plant bypasses sewage treatment and reaches the same discharge channel. The water manager, AMAP S.p.A., is willing to recover the energy from this head jump by installing a hydraulic turbine to reduce the energy costs linked to the treatment processes.

UL-PRS Turbine Solution

The design parameters chosen for the UL-PRS are a flow rate and a head drop, respectively, equal to 0.840 m³/s and 3.75 m. The available hydraulic jump $\Delta H = 3.75$ m is given by the difference between the Total Energy Level T.E.L.₁ of the inlet channel (with

respect to the bed of the discharge channel) and the T.E.L.₂ of the discharge channel, minus about 0.2 m of head losses ΔH_{ls} , estimated in the suction pipe and in the butterfly valve, respectively, marked with 3 and 4 in Figure 12. Following the design criteria discussed in [9–13], a diameter D and width W equal to 913 mm and 609 mm are selected, respectively, for a rotational velocity ω equal to 75 rpm. The UL-PRS turbine (marked with 6 in Figure 12) is installed in a specific underground room downstream of the plant channel. In the case of overflow, part of the water bypasses the turbine and reaches the discharge channel through the original rectangular weirs (green dashed arrows). In the case of maintenance work of the turbine, it is possible to cut off the turbine and restore the actual layout of the WWTP just by closing the butterfly valve and the gate valve, marked with numbers 4 and 7, respectively.

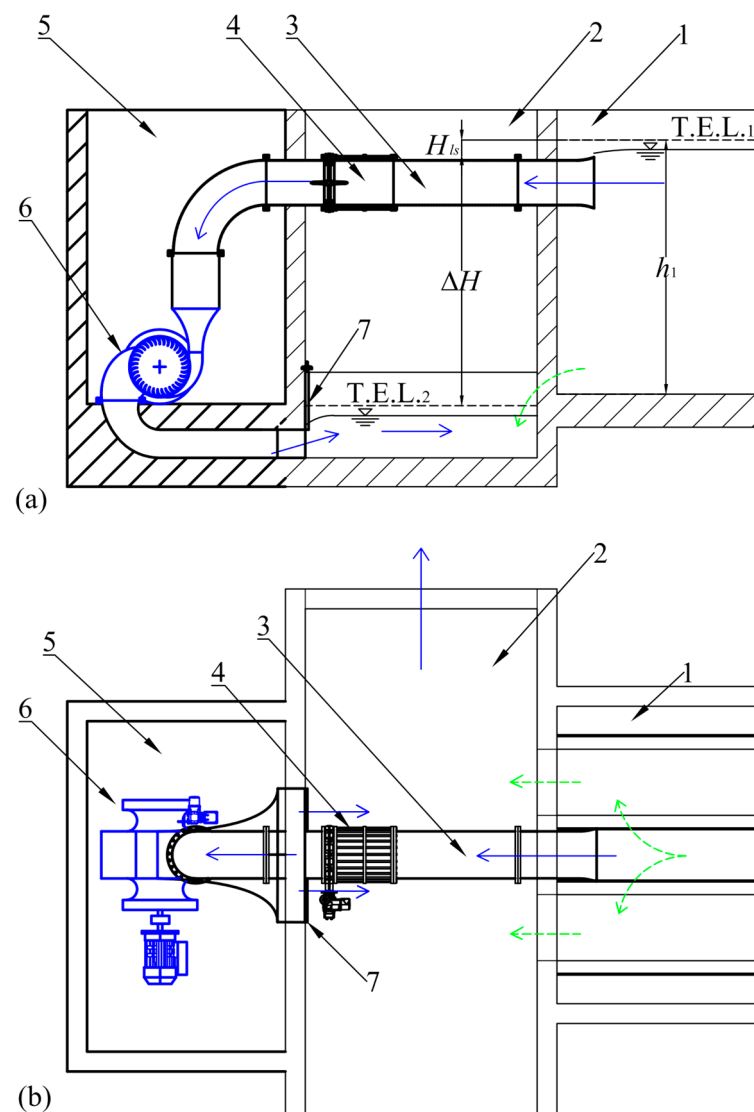


Figure 12. (a) Section and (b) planimetric view of a UL-PRS type turbine plant, where: 1. Inlet channel; 2. Discharge channel; 3. Suction pipe; 4. Butterfly valve; 5. Underground room; 6. T Hydropower System (blue lines); 7. Gate valve. In thick solid lines, the modifications are proposed for the new solution.

The iron pipe, with a circular section of diameter D_{pipe} equal to DN700, is connected to the rectangular inlet section of the nozzle of the turbine through a special convergent. 3D numerical analysis has been carried out for validation by computing the efficiency and the flow rate of the turbine for a given head drop ΔH . The turbine shows an efficiency

equal to 80.8%, with a mass flow rate close to the design data ($Q = 806 \text{ m}^3 \text{ s}^{-1}$; $\Delta H = 3.75 \text{ m}$; $\omega = 75 \text{ rpm}$; $\alpha = 15^\circ$; $\lambda_{\max} = 100^\circ$; $D = 913 \text{ mm}$; $W = 609 \text{ mm}$).

A comparison between the velocity fields in the symmetry plane of the 3D simulation (Figure 13a) and the 2D simulation (Figure 13b) shows a good match for the accuracy required by the proposed UL-PRS design approach, except for the last part of the diffuser, whose width increases with a hyperbolic law in the 3D model, whereas it is constant in the 2D analysis.

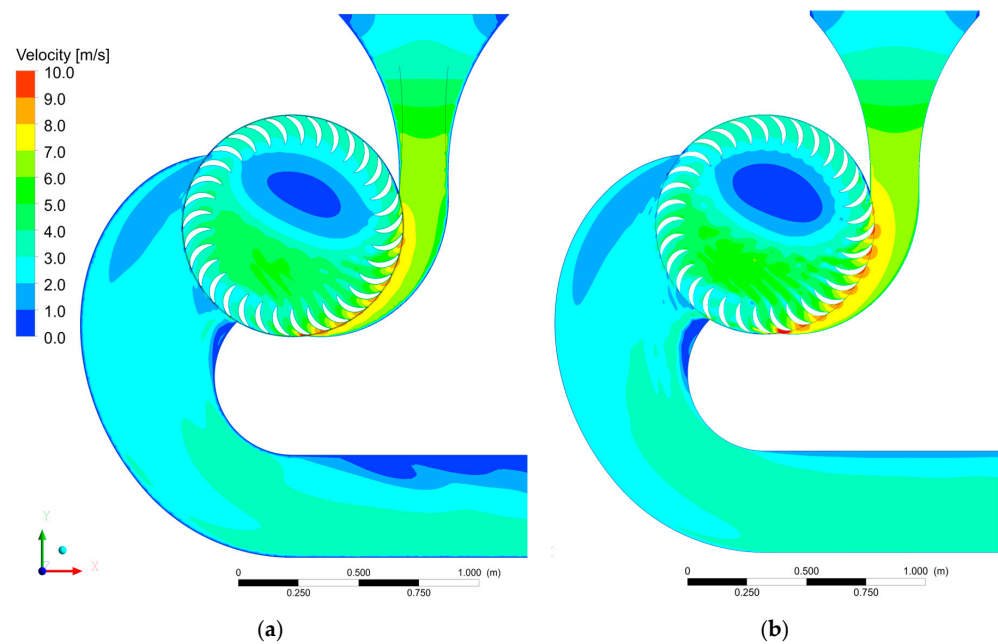


Figure 13. Velocity field of UL-PRS: (a) 3D and (b) 2D simulations.

Figure 14a,b show the head field, respectively, in the symmetry plane of the 3D simulation and the 2D one. From this comparison, similar conclusions can be derived.

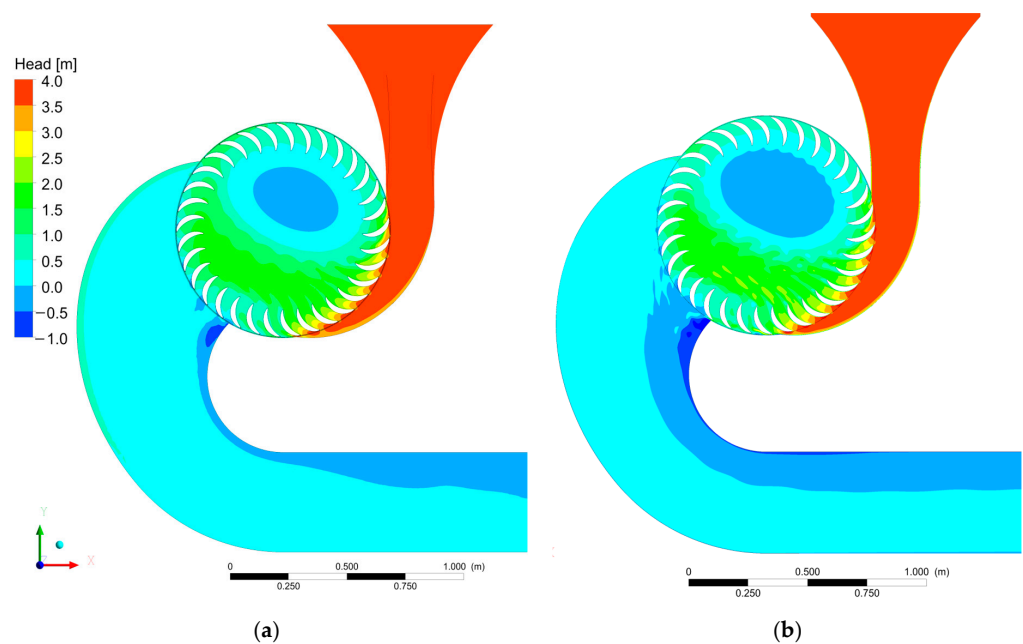


Figure 14. T.E.L. of UL-PRS: (a) 3D and (b) 2D.

See in Figures 15 and 16 3D views of the 3D solution.

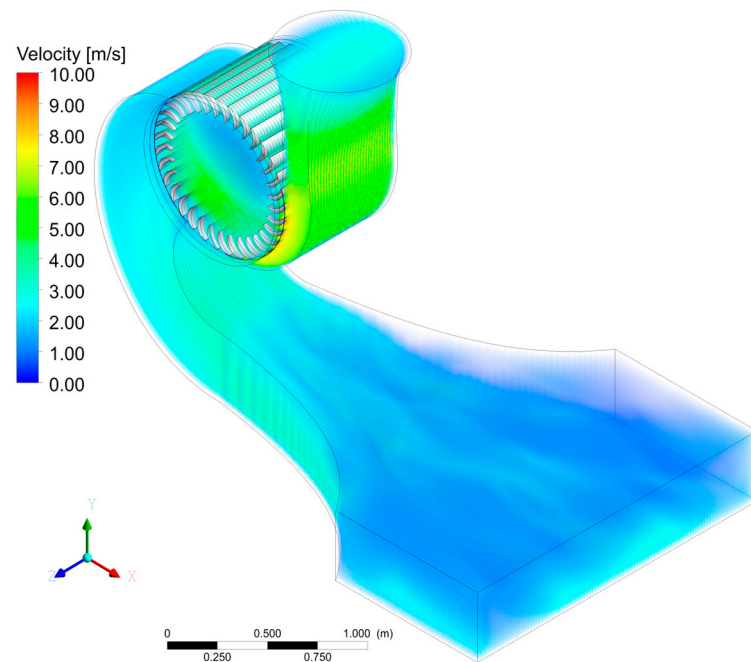


Figure 15. Velocity field of UL-PRS in 3D view.

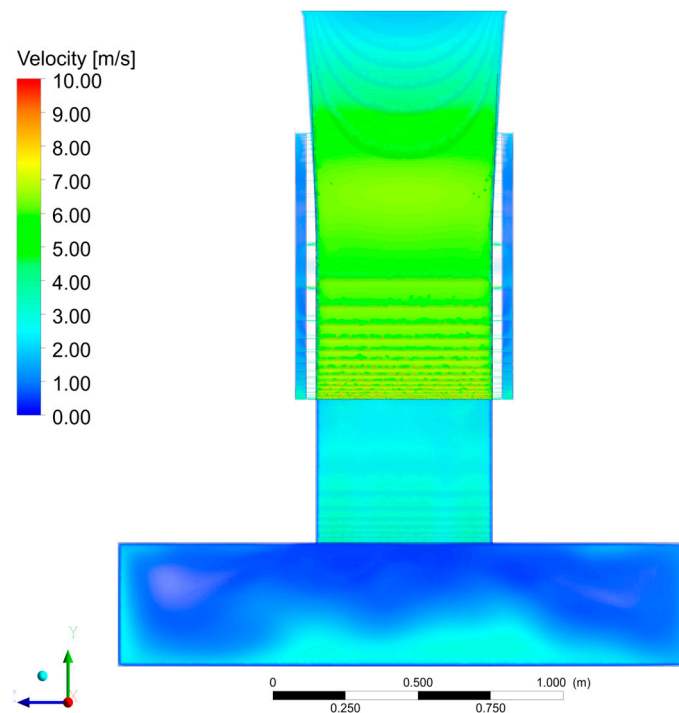


Figure 16. Velocity field in a frontal view of UL-PRS.

4. Cost/Benefit Analysis

An economic analysis is necessary to evaluate whether the new UL-PRS scheme should be chosen as an alternative to other possible schemes of hydropower systems. These schemes are compared on the basis of the expected costs and benefits during the lifespan of the turbine by means of economic criteria. Economic analysis strongly depends on the accuracy of the estimated costs and benefits. These estimations are not always easy to obtain, especially when some of the sought-after characteristics are only preliminarily defined.

The benefit for investors is savings in terms of self-produced energy or annual income from the sale of energy production. This benefit depends on the amount of energy produced during the lifespan of the turbine and on the specific conditions of the energy market.

It is useful to split the costs into the following main groups, as described below:

- Civil work costs: costs for the required modification of the existing infrastructure (black solid, thick lines in Figure 12). These costs include the excavation and building of a specific underground room downstream of the plant channel for turbine housing.
- Hydropower system costs: these include the cost of the turbine, the gearbox, and the electrical generator of an asynchronous type (Figure 12). We estimated a cost of 13,000 EUR for both the gearbox and the electrical generator with a high number of polar couples. For the UL-PRS turbine realization, we estimated a cost of 2500 EUR/kW.
- Control system and installation costs: these include the cost of the control system for the regulation and management of the turbine and the cost of installation. In the range of the investigated nominal electrical power ($P_e < 20$ kW), the control system cost can be expected to be equal to 40,000 EUR [15].
- Operation and maintenance (O&M) costs: in the case of micro hydro plants, the literature suggests assuming a yearly cost in the range of 2.2% to 3% of the cost of investment C_i [19].

$$C_{O\&Mmin} = 2.2\% C_i \text{ [EUR/year]} \quad (11)$$

$$C_{O\&Mmax} = 3.0\% C_i \text{ [EUR/year]} \quad (12)$$

Decommissioning costs are marginal compared to the other costs, also because part of these costs is compensated from recovery and sale of raw materials, such as copper, steel and other precious metals, present in the dismissing components. For this reason, they are neglected in the benefit/cost analysis.

In Table 4, we compare the UL-PRS solution with the installation of a commercial Kaplan Turbine and cross-flow turbine (CFT), assuming two possible different O&M annual costs (2.2% and 3.0% of C_i) [19]. For the evaluation of the Kaplan and CFT solution costs, we refer to [15].

Table 4. Comparison of economic indicators.

Parameters	UL-PRS	Kaplan *	CFT *
Head ΔH [m]	3.75	3.75	2.8
Flow rate Q [m ³ /s]	0.806	0.837	0.820
Hydraulic Efficiency	0.808	0.864	0.835
Gearbox/belts/generator efficiency	0.887	0.887	0.887
Global efficiency	0.717	0.766	0.741
Nominal Power (P_e) [kW]	21.2	23.6	16.7
Civil works [€]	20,000	20,000	20,000
Hydropower System [€]	66,000	165,000	50,000
Control system and installation [€]	40,000	40,000	40,000
Total cost (C_i) [€]	126,000	225,000	110,000
Specific cost [€/kW]	5943	9534	6587
O&M cost ($C_{O\&Mmin}-C_{O\&Mmax}$) [€/year]	2772–3780	4950–6750	2420–3300
Total producible energy [MWh]	178.080–167.904	198.240–186.912	140.280–132.264
Average cash flows (C_f) [€/year]	25,525–22,900	26,550–22,950	19,870–17,717
Payback period (n_y) [year]	4.9–5.5	8.5–9.8	5.5–6.2

* According to [15].

For hydropower plants with nominal power up to 1 MW and produced energy up to 250 MWh/year, the Italian Regulatory Authority for Energy Networks and Environment

(ARERA) sets a guaranteed minimum price p_{MWh} for the sale of energy. This guaranteed minimum price p_{MWh} is equal to 158.9 EUR /MWh for 2022 [20].

The total energy to be produced over a typical year and the corresponding average cash flows are calculated assuming the hydropower plant to be working 24 h per day and 350 or 330 days per year, respectively, in the case of O&M cost equal to $C_{O\&Mmin}$ or $C_{O\&Mmax}$ (Table 4). A single index well representing the global economic benefit of the plant is the payback period n_y [years], given by the ratio between the cost of investment C_i [€] and the average cash flows C_f [€/year] of each solution in both cases of $C_{O\&Mmin}$ or $C_{O\&Mmax}$.

$$C_f = \frac{P_e}{1000} \cdot 24 \text{ h} \cdot \text{days} \cdot p_{MWh} - C_{o\&M} [\text{EUR}/\text{year}] \tag{13}$$

$$n_y = \frac{C_i}{C_f} [\text{years}] \tag{14}$$

The UL-PRS plant is the solution with the shorter payback period (Table 4). Other indices to be taken into account for device selection are the risk of cavitation due to unexpected flow rates, as well as the constructive simplicity of the device and the corresponding low maintenance cost. A more detailed cost analysis could also explicitly account for the temporal variation in money value.

A summary of all the benefits of each solution is reported in Table 5.

Table 5. Benefit comparison of solutions.

	UL-PRS	Kaplan *	CFT *
Entire available hydraulic jump	✓	✓	✗
Risk of cavitation	✗	✗	✓
Hydraulic Efficiency > 80%	✓	✓	✓
Payback period	✓	✗	✗
Nominal Power > 20 kW	✓	✓	✗
Constructive simplicity of the turbine	✓	✗	✓

* According to [15].

5. Conclusions

For low head jumps, Kaplan type turbines attain efficiency higher than 85% and are traditionally assumed to be the most efficient ones, but the results shown in the present analysis suggest that the new UL-PRS type turbine could also be an attractive alternative solution. The main advantage of UL-PRS and CFT turbines is their constructive simplicity; moreover, their cost could be, for the same nominal power, much lower than the cost of Kaplan turbines. The pressurized outflow present in UL-PRS allows, in contrast to CFT turbines, exploitation of the entire available hydraulic jump, still saving a global efficiency greater than 80%.

UL-PRS turbines show an abrupt reduction in efficiencies for head drops lower than 0.5 m. Further research is still required in this head range to optimize the shape of the stator and the rotor when the velocity of the particles entering the rotor significantly changes from one point to another on the inlet surface.

Author Contributions: Conceptualization: M.S. and T.T.; Investigation and Data Curation: C.P. and L.G.; Software: C.P. and M.S.; Writing—Review & Editing: C.P., M.S. and L.G.; Formal Analysis: P.G.F.F.; Supervision: T.T. and P.G.F.F. All authors have read and agreed to the published version of the manuscript.

Funding: This research has been carried out as part of the contract n. 9794 of 09/09/2021 between the University Mediterranea of Reggio Calabria and the Regione Calabria, with the financial support of Regione Calabria.

Institutional Review Board Statement: Not applicable.

Informed Consent Statement: Not applicable.

Data Availability Statement: Not applicable.

Conflicts of Interest: The authors declare no conflict of interest.

Abbreviations

ARERA	Italian Regulatory Authority for Energy, Networks and Environment
BCs	Boundary conditions
CFD	Computational Fluid Dynamics
CFT	Cross-flow Turbine
E_{inH}	Equivalent Inhabitants
H-PRS	High Power Recovery System
PRS	Power Recovery System
O&M	Operation and Maintenance
T.E.L.	Total Energy Level
UL-PRS	Ultra-low Power Recovery System
WWTP	Wastewater Treatment Plant

Symbols

C_i	total cost (EUR)
C_f	average cash flows (EUR/Year)
$C_{O\&Mmin}$	minimum operation and maintenance annual cost (EUR/Year)
$C_{O\&Mmax}$	maximum operation and maintenance annual cost (EUR/Year)
D	outer runner diameter (m)
D_{pipe}	diameter of the pipe (m)
ΔH	specific energy drop per unit weight (m)
g	standard acceleration due to gravity ($m\ s^{-2}$)
k	constant in linear law of the velocity (s^{-1})
l	distance from the beginning of part III (m)
l_{max}	length of part III of the diffuser (m)
N_b	number of blades (–)
n_y	payback period (years)
P	produced mechanical power of the turbine (W)
P_e	nominal electrical power (kW)
p	pressure plus the geodetic term (Pa)
p'	value of pressure (Pa)
p_{MWh}	guaranteed minimum prices for the sale of energy (EUR/MWh)
Q	mass flow rate ($m^3\ s^{-1}$)
R	outer runner radius (m)
$r(\lambda)$	radial distance r of the profile of the external wall of the diffuser from the axis of the rotor (m)
S_{max}	maximum height of the diffuser in part I (m)
t	blade thickness (m)
t_{max}	blade maximum thickness (m)
$V(l)$	generic velocity of particles in part III ($m\ s^{-1}$)
V_0	velocity at the beginning of part III ($m\ s^{-1}$)
V_2	runner outlet velocity ($m\ s^{-1}$)
V_{out}	velocity at the end of part III ($m\ s^{-1}$)
W	runner width (m)
$W(l)$	generic width of part III of the diffuser (m)
W_{out}	maximum width of part III of the diffuser (m)
y	geodetic elevation respect the axis of the runner (m)
α	absolute velocity inlet angle (radians)
β	relative velocity inlet angle (radians)
γ	water specific weight ($N\ m^{-3}$)
η	hydraulic efficiency of the turbine (–)

η	normalized hydraulic efficiency of the turbine (–)
λ	runner inlet/outlet angle (radians)
λ_{\max}	maximum runner angle (radians)
ρ	density of the water (kg m^{-3})
ρ_0	density of the air at 15 °C (kg m^{-3})
ω	runner rotational velocity (rad s^{-1})

References

- Damtew, Y.; Getenet, G. Assessment of Hydropower Potential of Selected Rivers in North Shoa Zone, Amhara Regional State, Ethiopia. *Am. J. Energy Res.* **2019**, *7*, 15–18. [[CrossRef](#)]
- Finger, D.; Schmid, M.; Wüest, A. Effects of upstream hydropower operation on riverine particle transport and turbidity in downstream lakes. *Water Resour. Res.* **2006**, *42*, W08429. [[CrossRef](#)]
- Kuriqi, A.; Pinheiro, A.N.; Sordo-Ward, A.; Garrote, L. Influence of hydrologically based environmental flow methods on flow alteration and energy production in a run-of-river hydropower plant. *J. Clean. Prod.* **2019**, *232*, 1028–1042. [[CrossRef](#)]
- Trussart, S.; Messier, D.; Roquet, V.; Aki, S. Hydropower projects: A review of most effective mitigation measures. *Energy Policy* **2002**, *30*, 1251–1259. [[CrossRef](#)]
- Scherer, L.; Pfister, S. Global water footprint assessment of hydropower. *Renew. Energy* **2016**, *99*, 711–720. [[CrossRef](#)]
- Li, Y. On the definition of the power coefficient of tidal current turbines and efficiency of tidal current turbine farms. *Renew. Energy* **2014**, *68*, 868–875. [[CrossRef](#)]
- Zhou, D.; Gui, J.; Deng, Z.D.; Chen, H.; Yu, Y.; Yu, A.; Yang, C. Development of an ultra-low head siphon hydro turbine using computational fluid dynamics. *Energy* **2019**, *181*, 43–50. [[CrossRef](#)]
- Guzmán-Avalos, P.; Molinero-Hernández, D.; Galván-González, S.; Herrera-Sandoval, N.; Solorio-Díaz, G.; Rubio-Maya, C. Numerical design and optimization of a hydraulic micro-turbine adapted to a wastewater treatment plant. *Alex. Eng. J.* **2023**, *62*, 555–565. [[CrossRef](#)]
- Sinagra, M.; Sammartano, V.; Morreale, G.; Tucciarelli, T. A New Device for Pressure Control and Energy Recovery in Water Distribution Networks. *Water* **2017**, *9*, 309. [[CrossRef](#)]
- Sinagra, M.; Aricò, C.; Tucciarelli, T.; Morreale, G. Experimental and numerical analysis of a backpressure Banki inline turbine for pressure regulation and energy production. *Renew. Energy* **2020**, *149*, 980–986. [[CrossRef](#)]
- Sinagra, M.; Aricò, C.; Tucciarelli, T.; Amato, P.; Fiorino, M. Coupled Electric and Hydraulic Control of a PRS Turbine in a Real Transport Water Network. *Water* **2019**, *11*, 1194. [[CrossRef](#)]
- Sammartano, V.; Sinagra, M.; Filianoti, P.; Tucciarelli, T. A Banki-Michell turbine for in-line hydropower systems. *J. Hydraul. Res.* **2017**, *55*, 686–694. [[CrossRef](#)]
- Sinagra, M.; Picone, C.; Aricò, C.; Pantano, A.; Tucciarelli, T.; Hannachi, M.; Driss, Z. Impeller Optimization in Crossflow Hydraulic Turbines. *Water* **2021**, *13*, 313. [[CrossRef](#)]
- Picone, C.; Sinagra, M.; Aricò, C.; Tucciarelli, T. Numerical analysis of a new cross-flow type hydraulic turbine for high head and low flow rate. *Eng. Appl. Comput. Fluid Mech.* **2021**, *15*, 1491–1507. [[CrossRef](#)]
- Sinagra, M.; Picone, C.; Picone, P.; Aricò, C.; Tucciarelli, T.; Ramos, H.M. Low-Head Hydropower for Energy Recovery in Wastewater System. *Water* **2022**, *14*, 1649. [[CrossRef](#)]
- Sammartano, V.; Aricò, C.; Carravetta, A.; Fecarotta, O.; Tucciarelli, T. Banki-Michell Optimal Design by Computational Fluid Dynamics Testing and Hydrodynamic Analysis. *Energies* **2013**, *6*, 2362–2385. [[CrossRef](#)]
- Picone, C. Recupero Energetico All'interno delle reti Acquedottistiche Mediante Microturbine Idrauliche. Ph.D. Thesis, Department of Engineering, Palermo University, Palermo, Italy, 2022.
- Aricò, C.; Sinagra, M.; Picone, C.; Tucciarelli, T. MAST-RT0 solution of the incompressible Navier–Stokes equations in 3D complex domains. *Eng. Appl. Comput. Fluid Mech.* **2021**, *15*, 53–93. [[CrossRef](#)]
- Alawadhi, G.; Almehiri, M.; Sakhrieh, A.; Alshwawra, A.; Al Asfar, J. Cost Analysis of Implementing In-Pipe Hydro Turbine in the United Arab Emirates Water Network. *Sustainability* **2023**, *15*, 651. [[CrossRef](#)]
- Italian Regulatory Authority for Energy, Networks and Environment (ARERA). Prezzi Minimi Garantiti per L'anno 2022. Available online: <https://www.arera.it/it/comunicati/22/220118.htm> (accessed on 18 January 2022).

Disclaimer/Publisher's Note: The statements, opinions and data contained in all publications are solely those of the individual author(s) and contributor(s) and not of MDPI and/or the editor(s). MDPI and/or the editor(s) disclaim responsibility for any injury to people or property resulting from any ideas, methods, instructions or products referred to in the content.